Biomacromolecules

pubs.acs.org/Biomac

Article

Glucose and Maltose Surface-Functionalized Thermoresponsive Poly(*N*-Vinylcaprolactam) Nanogels

Joonas Siirilä, Sami Hietala, Filip S. Ekholm, and Heikki Tenhu*

Cite This: *Biomacromolecules* 2020, 21, 955−965

Read Online

ACCESS | Metrics & More | Article Recommendations | Supporting Information

ABSTRACT: Soft nanoparticles are interesting materials due to their size, deformability, and ability to host guest molecules. Surface properties play an essential role in determining the fate of the particles in biological medium, and coating of the nanoparticles (and polymers) with carbohydrates has been found to be an efficient strategy for increasing their biocompatibility and fine-tuning other important properties such as aqueous solubility. In this work, soft nanogels of poly(*N*-vinylcaprolactam), PNVCL, were surface-functionalized with different glucose and maltose ligands, and the colloidal properties of the gels were analyzed. The PNVCL nanogels were first prepared via semibatch precipitation polymerization, where a comonomer, propargyl acrylate (PA), was added after preparticle formation. The aim was to synthesize "clickable" nanogels with alkyne groups on their surfaces. The nanogels were then functionalized with two separate azido-glucosides and azido-maltosides (containing different linkers) through a copper-catalyzed azide−alkyne cycloaddition (CuAAc) click reaction. The glucose and maltose bearing nanogels were thermoresponsive and shrank upon heating. Compared to the PNVCL−PA nanogel, the carbohydrate bearing ones were larger, more hydrophilic, had volume phase transitions at higher temperatures, and were more stable against salt-induced precipitation. In addition to investigating the colloidal properties of the nanogels, the carbohydrate recognition was addressed by studying the interactions with a model lectin, concanavalin A (Con A). The binding efficiency was not affected by the temperature, which indicates that the carbohydrate moieties are located on the gel surfaces, and are capable of interacting with other biomolecules independent of temperature. Thus, the synthesis produces nanogels, which have surface functions capable of biorelevant interactions and a thermoresponsive structure. These types of particles can be used for drug delivery.

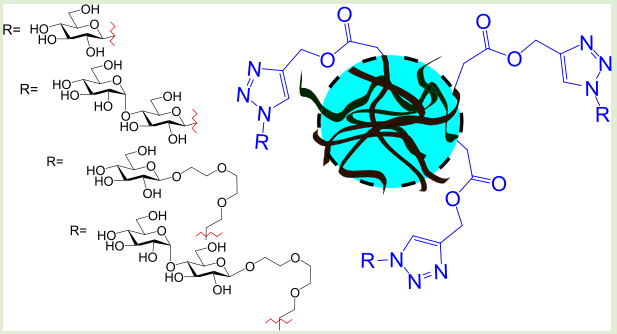

INTRODUCTION

Nanogels are solvent-swollen polymer networks with sizes ranging from nanometers to hundreds of nanometers. The gel particles are soft, deformable, and penetrable, and when comprised of amphiphilic polymers, they have surface-active properties. The particles are suitable for utilization as nanoreactors, stabilizers, biomimetic systems, and as carriers for desired substances.[1−3] Many of these gels are also stimuli-responsive and as such attractive building blocks for smart systems, including on−off catalysts,[4] emulsions that can be separated with a trigger,[5] and on-demand[6] or on-site[7] cargo release systems. Typical stimuli include light, radio-frequency (RF), temperature, pressure, ion concentration, and pH. A typical response to stimuli is a change in the conformation and solubility of the polymer, which results in a volume change of the gel.

Poly(*N*-vinylcaprolactam), PNVCL, is a versatile polymer, which exhibits thermoresponsive behavior in water.[8] The polymer is soluble in cold water and becomes insoluble upon heating. It is an attractive polymer for nanogels due to being nontoxic, compatible with many guest molecules (hydrophobic interactions, H-bonds), and because the thermal transition temperature is close to the human body temperature. PNVCL nanogels have already proven to exhibit antiviral activity against HIV-virus[9] and have been studied as drug delivery systems.[7,10−13] In biomedical applications, the surface properties of the nanogels are essential, and for all materials intended for human use, the interactions with other types of biomolecules are important. A way to control such interactions is to tune the surface functionality through chemical modification.

The synthesis of surface-functionalized PNVCL nanogels can be performed through a semibatch precipitation polymerization, which typically produces core−shell particles.[14] Previously, this method has been applied to the synthesis of PNVCL nanogels using glycidyl methacrylate, GMA,[15] or propargyl acrylate, PA,[16] as comonomers. The GMA or PA groups, which reside on the surface of the nanogels can be

Received: November 21, 2019
Revised: January 7, 2020
Published: January 9, 2020

further functionalized through postpolymerization reactions. The epoxy-groups on GMA are reactive toward nucleophiles such as carboxylic acids, amines, and thiols, while the alkyne groups of PA can be functionalized via click chemistry, i.e., thiol-yne or copper-catalyzed alkyne−azide cycloaddition (CuAAC) reactions.[17,18]

In the current work, our aim was to synthesize carbohydrate-containing PNVCL nanogels and evaluate the effects of functionalization on the colloidal properties of the end products while simultaneously briefly addressing biological aspects. In more detail, PNVCL-based nanogels (PNVCL−PA nanogels) carrying propargyl moieties were synthesized and postpolymerization functionalized with azido-glucosides and azido-maltosides (Figure 1). Modifying a nanoparticle surface

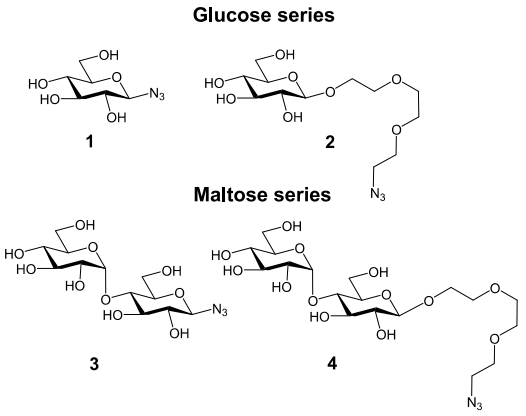

Figure 1. Molecular structures of the carbohydrate azides **1**−**4** used in this study. The following names will be used **1**: Glc-N_3; **2**: Glc-TEG-N_3; **3**: Mal-N_3; and **4**: Mal-TEG-N_3.

with carbohydrates is a promising general strategy for increasing their hydrophilicity and biocompatibility.[19] In addition, the carbohydrates play important roles in biological recognition events, e.g., in cell−cell adhesion and communication processes.[20] In fact, in many of the application areas in which PNVCL nanogels are envisioned to be of importance, their properties could benefit from carbohydrate coating (drug delivery, biomimetic systems, and biomolecule scavenging/sensing). The examples on carbohydrate-modified hydrogel particles are limited in the literature,[21−31] and only a few examples of PNVCL hydrogel particles bearing carbohydrates can be found.[23,29] Herein, we opted to modify the PNVCL hydrogel particle surfaces with glucosides and maltosides bearing different linker lengths and examine the effects on the structural and colloidal properties of the end products. The carbohydrates were chosen because glucose and its glycopolymers are widely used by organisms, and maltosides have recently been shown to bind to the noncanonical binding site of galectin-3,[32] a lectin that plays an important role in innate immunity.[33] Therefore, to evaluate if the carbohydrates on the PNVCL nanogels would be accessible to interact with biomolecules, a preliminary binding assay featuring a plant-based lectin, Concanavalin A (Con A), was conducted.

EXPERIMENTAL SECTION

Materials. All reagents were from commercial sources and used as such if not stated otherwise. Methacrylic acid (MAA) and propargyl acrylate (PA) were purified via column chromatography using an inhibitor remover resin. NVCL was recrystallized twice from toluene. *N*,*N*′-bis(acryloyl)cystamine (BAC) was synthesized according to the literature protocol.[34] The carbohydrate ligand for solubilizing copper (I) in water was synthesized according to a literature protocol.[35] The lectin concanavalin A, Con A, from Canavalia Ensiformis (Jack Bean), Type VI, M = 25 500 g/mol was obtained as a lyophilized powder. Lectin solutions were prepared by first dissolving lectin in aqueous 10 mM 4-(2-hydroxyethyl)-1-piperazineethanesulfonic acid (HEPES, pH = 7.4) buffer (1 mg/mL) and then removing the nondissolved residue by centrifugation at room temperature. The concentration of solutions was determined from UV absorption at 278 nm.

Synthesis of Carbohydrate Azides. All reactions containing moisture- or air-sensitive reagents were carried out under an argon atmosphere. Reaction solvents were purified by the VAC vacuum solvent purification system prior to use when dry solvents were needed. The nuclear magnetic resonance (NMR) spectra were recorded using a Bruker Avance III NMR spectrometer (^{1}H: 500.13 MHz, ^{13}C: 125.76 MHz). The probe temperature during the experiments was kept at 23 °C. All products of the carbohydrate azide synthesis were characterized by utilization of the following one-dimensional (1D) techniques: ^{1}H and ^{13}C and the following two-dimensional (2D) techniques: correlation spectroscopy (COSY), total correlated spectroscopy (TOCSY), multiplicity-edited heteronuclear single quantum correlation (Ed-HSQC) and heteronuclear multiple bond coherence (HMBC) using pulse sequences provided by the instrument manufacturer. Chemical shifts are expressed on the δ scale (in ppm) using tetramethylsilane (TMS) or residual solvents as internal standards. Coupling constants are given in Hertz and provided only once when first encountered. Coupling patterns are given as singlet (s), doublet (d), triplet (t), etc. HRMS were recorded using Bruker Micro Q-TOF with electrospray ionization (ESI) operated in positive mode. During the reactions, the reaction progress was monitored with a Bruker Ultraflex III matrix-assisted laser desorption ionization-time-of-flight (MALDI-TOF) mass spectrometer operated in positive mode. Thin-layer chromatography (TLC) was performed on aluminum sheets precoated with silica gel 60 F254 (Merck). Flash chromatography was carried out on silica gel 40. Spots were visualized by spraying the TLC plates with a 1:4 H_2SO_4/MeOH-mixture followed by heating.

1-Azido-1-deoxy-β-D-glucopyranoside (Glc-N_3). 2,3,4,6-Tetra-*O*-acetyl-α-D-glucopyranosyl bromide (2.1 g, 4.8 mmol) was dissolved in dry dimethylformamide (DMF) (20 mL), and NaN_3 (0.95 g, 14.5 mmol, 3 equiv) was added. The resulting mixture was stirred at 55 °C for 2.5 h and cooled to room temperature (r.t.). The reaction mixture was diluted with EtOAc (40 mL) and washed with saturated $NaHCO_3$ solution (30 mL), H_2O (30 mL), and brine (30 mL). The organic phase was separated, dried over Na_2SO_4, and concentrated. The crude product was purified by column chromatography (Hexane/EtOAc 1:1) to give 1-azido-1-deoxy-2,3,4,6-tetra-*O*-acetyl-β-D-glucopyranoside as a white solid (1.5 g, 83%).

^{1}H NMR (500.13 MHz, $CDCl_3$ + TMS): δ 5.22 (ap t, 1H, $J_{3,2}$ = 9.6, $J_{3,4}$ = 9.6 Hz, H-3), 5.11 (ap t, 1H, $J_{4,5}$ = 9.6 Hz, H-4), 4.96 (dd, 1H, $J_{2,1}$ = 8.8 Hz, H-2), 4.65 (d, 1H, H-1), 4.28 (dd, 1H, $J_{6a,5}$ = 4.9, $J_{6a,6b}$ = −12.5 Hz, H-6a), 4.18 (dd, 1H, $J_{6b,5}$ = 2.3 Hz, H-6b), 3.80 (ddd, 1H, H-5), 2.11 (s, 3H, 6-OCOCH_3), 2.08 (s, 3H, 2-OCOCH_3), 2.04 (s, 3H, 4-OCOCH_3), and 2.01(s, 3H, 3-OCOCH_3) ppm.

^{13}C NMR (125.76 MHz, $CDCl_3$ + TMS): δ 170.7 (6-$OCOCH_3$), 170.3 (3-$OCOCH_3$), 169.4 (4-$OCOCH_3$), 169.3 (2-$OCOCH_3$), 88.1 (C-1), 74.2 (C-5), 72.7 (C-3), 70.8 (C-2), 68.0 (C-4), 61.8 (C-6), 20.8 (3-$OCOCH_3$), and 20.7 (2-$OCOCH_3$, 4-$OCOCH_3$, 6-$OCOCH_3$) ppm.

HRMS: calculated for $C_{14}H_{19}O_9N_3Na$, $[M + Na]^+$: 396.101 and measured: 396.151.

1-Azido-1-deoxy-2,3,4,6-tetra-*O*-acetyl-β-D-glucopyranoside (0.91 g, 2.4 mmol) was dissolved in dry MeOH (25 mL) and the pH was raised to 10 with a NaOMe solution (5 M in MeOH). The mixture was stirred overnight, neutralized with AG 50 (H^+-form), filtered, and concentrated. The crude product was purified by column chromatography (CH_2Cl_2/MeOH 3:1) to give the title compound as a colorless oil (0.45 g, 92%).

^{1}H NMR (500.13 MHz, D_2O): δ 4.74 (d, 1H, $J_{1,2}$ = 8.8 Hz, H-1), 3.91 (dd, 1H, $J_{6a,5}$ = 2.2, $J_{6a,6b}$ = −12.4 Hz, H-6a), 3.74 (dd, 1H, $J_{6b,5}$ =

https://dx.doi.org/10.1021/acs.biomac.9b01596
Biomacromolecules 2020, 21, 955−965

5.7 Hz, H-6b), 3.53 (ddd, 1H, $J_{5,4}$ = 9.9 Hz, H-5), 3.51 (ap t, 1H, $J_{3,2}$ = 9.3, $J_{3,4}$ = 9.3 Hz, H-3), 3.41 (dd, 1H, H-4), and 3.26 (dd, 1H, H-2) ppm.

^{13}C NMR (125.76 MHz, D_2O): δ 90.1 (C-1), 77.8 (C-5), 75.7 (C-3), 72.8 (C-2), 69.1 (C-4), and 60.5 (C-6) ppm.

HRMS: calculated for $C_6H_{11}O_5N_3Na$, $[M + Na]^+$: 228.059 and measured: 228.055.

2-[2-(2-Azidoethoxy)ethoxy]ethyl β-D-glucopyranoside (Glc-TEG-N$_3$). Peracetylated D-glucose (2.8 g, 7.1 mmol) was dissolved in dry CH_2Cl_2 (20 mL, under an argon atmosphere). 2-[2-(2-Chloroethoxy)ethoxy]ethanol (4 mL, 28 mmol, 4 equiv) was added to the solution, and the reaction mixture was cooled on an ice bath. $BF_3{\cdot}OEt_2$ (6.8 mL, 55 mmol, 8 equiv) was added dropwise, and the reaction mixture was slowly warmed to r.t. and left to stir for 5 h (MALDI-TOF analysis was utilized to monitor the reaction progress: $[M + Na]^+$ calculated for $C_{20}H_{31}ClO_{12}Na$: 521.140; observed: 521.309). The reaction mixture was cooled on an ice bath and neutralized with Et_3N. The mixture was brought to r.t., diluted with CH_2Cl_2 (30 mL), and washed with saturated $NaHCO_3$ solution (30 mL) and brine (30 mL). The organic phase was separated, dried over Na_2SO_4, filtered, and concentrated. The crude product was partially purified by column chromatography (EtOAc/hexane 2:1) to give an oil (2.2 g). The partially purified product was utilized as such in the following step.

The oil (2.2 g, 4.4 mmol) was dissolved in dry DMF (20 mL), and Bu_4NI (1.6 g, 4.3 mmol, ∼1 equiv) and NaN_3 (1.4 g, 22 mmol, ∼5 equiv) were added. The resulting mixture was refluxed at 87 °C overnight (MALDI-TOF analysis was utilized to monitor the reaction progress; $[M + Na]^+$ calculated for $C_{20}H_{31}N_3O_{12}Na$: 528.180; observed: 528.377) and concentrated. The crude product was filtered through a pad of silica (EtOAc) (impurities still present). The partially purified product was utilized as such in the following step.

The crude product was dissolved in dry MeOH (10 mL), and the pH was adjusted to 10−11 with a 5 M NaOMe solution. TLC-monitoring ($MeOH/CH_2Cl_2$ 1:5) of the reaction progress indicated that the reaction was complete after 2.5 h. The reaction mixture was neutralized with AG 50-X8 (H^+-form), diluted with MeOH (20 mL), filtered, and concentrated to give the crude product. The crude product was purified by column chromatography ($MeOH/CH_2Cl_2$ 1:9→1:3) to give the title compound as a white foam (0.33 g, 0.98 mmol, β/α 95:5, yield over three steps: 14%).

^{1}H NMR of the β-anomer (500.13 MHz, D_2O): δ 4.49 (d, 1H, $J_{1,2}$ = 8.0 Hz, H-1), 4.07 (ap dt, $J_{L1a,L2}$ = 4.03, $J_{L1a,Lb}$ = −11.6 Hz, H-L1a), 3.91 (dd, 1H, $J_{6a,5}$ = 2.2, $J_{6a,6b}$ = −12.4 Hz, H-6a), 3.84 (m, 1H, H-L1b), 3.78−3.72 (m, 8H, H-L2 (both), H-L3 (both), H-L4 (both), H-L5 (both)), 3.71 (dd, 1H, $J_{6b,5}$ = 6.0 Hz, H-6b), 3.53−3.48 (m, 3H, H-L6 (both), H-3), 3.45 (ddd, 1H, $J_{5,4}$ = 9.8 Hz, H-5), 3.38 (dd, 1H, $J_{4,3}$ = 9.1 Hz, H-4), and 3.29 (dd, 1H, H-2) ppm.

^{13}C NMR of the β-anomer (125.76 MHz, D_2O): δ 102.2 (C-1), 75.9 (C-5), 75.6 (C-3), 73.1 (C-2), 69.7−69.1 (C-L2, C-L3, C-L4, C-L5, C-4), 68.7 (C-L1), 60.7 (C-6), and 50.1 (C-L6).

HRMS: calculated for $C_{12}H_{23}O_8N_3Na$, $[M + Na]^+$: 360.138 and measured: 360.308.

1-Azido-1-deoxy-(α-D-glucopyranosyl)-(1→4)-β-D-glucopyranoside (Mal-N$_3$). Acetobromo-α-maltose (2.51 g, 3.6 mmol) was dissolved in dry DMF (15 mL), and NaN_3 (0.71 g, 10.9 mmol, 3 equiv) was added. The resulting mixture was stirred at 60 °C for 2.5 h and cooled to r.t. The reaction mixture was diluted with EtOAc (40 mL) and washed with saturated $NaHCO_3$ solution (30 mL), H_2O (30 mL), and brine (30 mL). The organic phase was separated, dried over Na_2SO_4, and concentrated. The crude product was purified by column chromatography (hexane/EtOAc 2:3) to give the peracetylated 1-azido-1-deoxy-(α-D-glucopyranosyl)-(1→4)-β-D-glucopyranoside as a colorless syrup (1.2 g, 50%).

^{1}H NMR (500.13 MHz, D_2O): δ 5.41 (d, 1H, $J_{1,2}$ = 4.0 Hz, H-1′), 5.36 (dd, 1H, $J_{3',4'}$ = 9.8, $J_{3',2'}$ = 10.4 Hz, H-3′), 5.26 (dd, 1H, $J_{3,4}$ = 9.0, $J_{3,2}$ = 9.1 Hz, H-3), 5.06 (dd, 1H, $J_{4',5'}$ = 9.9 Hz, H-4′), 4.86 (dd, 1H, H-2′), 4.78 (dd, 1H, $J_{2,1}$ = 8.7 Hz, H-2), 4.71 (d, 1H, H-1), 4.51 (dd, 1H, $J_{6a,5}$ = 2.6, $J_{6a,6b}$ = −12.2 Hz, H-6a), 4.25 (dd, 1H, $J_{6b,5}$ = 4.5 Hz, H-6b), 4.25 (dd, 1H, $J_{6'a,5'}$ = 3.7, $J_{6'a,6'b}$ = −12.3 Hz, H-6′a), 4.05 (dd, 1H, $J_{6'b,5'}$ = 2.3 Hz, H-6′b), 4.02 (dd, 1H, $J_{4,5}$ = 9.4 Hz, H-4), 3.96 (ddd, 1H, H-5′), 3.79 (ddd, 1H, H-5), 2.16 (6-OCOCH_3), 2.11 (6′-OCOCH_3), 2.05 (2-OCOCH_3), 2.04 (2′-OCOCH_3), 2.03 (4′-OCOCH_3), 2.02 (3-OCOCH_3), and 2.00 (3′-OCOCH_3) ppm.

^{13}C NMR (125.76 MHz, D_2O): δ 170.7 (2′-OCOCH_3, 6′-OCOCH_3), 170.5 (6-OCOCH_3), 170.2 (3-OCOCH_3), 170.1 (3′-OCOCH_3), 169.6 (2-OCOCH_3, 4′-OCOCH_3), 95.9 (C-1′), 87.6 (C-1), 75.2 (C-3), 74.4 (C-5), 72.5 (C-4), 71.7 (C-2), 70.1 (C-2′), 69.4 (C-3′), 68.8 (C-5′), 68.1 (C-4′), 62.7 (C-6), 61.6 (C-6′), and 21.0−20.7 (2′-OCOCH_3, 3′-OCOCH_3, 4′-OCOCH_3, 6′-OCOCH_3, 2-OCOCH_3, 3-OCOCH_3, 6-OCOCH_3) ppm.

HRMS: calculated for $C_{26}H_{35}O_{17}N_3Na$, $[M + Na]^+$: 684.186 and measured: 684.188.

The colorless syrup (0.8 g, 1.2 mmol) was dissolved in dry MeOH (10 mL) and the pH was raised to 10 with a NaOMe solution (5 M in MeOH). The mixture was stirred for 4 h, neutralized with AG 50 (H^+-form), filtered, and concentrated. The crude product was purified by column chromatography (CH_2Cl_2/MeOH 2:1) to give the title compound as a colorless syrup (0.39 g, 88%).

^{1}H NMR (500.13 MHz, D_2O): δ 5.44 (d, 1H, $J_{1,2}$ = 3.9 Hz, H-1′), 4.78 (d, 1H, $J_{1,2}$ = 8.8 Hz, H-1), 3.97 (dd, 1H, $J_{6a,5}$ = 1.0, $J_{6a,6b}$ = −12.4 Hz, H-6a), 3.88 (dd, 1H, $J_{6'a,5'}$ = 2.2, $J_{6'a,6'b}$ = −12.3 Hz, H-6′a), 3.83 (dd, 1H, $J_{3,4}$ = 9.0, $J_{3,2}$ = 9.1 Hz, H-3), 3.82 (dd, 1H, $J_{6b,5}$ = 4.5 Hz, H-6b), 3.79 (dd, 1H, $J_{6'b,5'}$ = 5.1 Hz, H-6′b), 3.74 (ddd, 1H, $J_{5',4'}$ = 9.9 Hz, H-5′), 3.73−3.67 (m, 3H, H-3′, H-4, H-5), 3.61 (dd, 1H, $J_{2',3'}$ = 10.0 Hz, H-2′), 3.44 (dd, 1H, $J_{4',3'}$ = 9.4 Hz, H-4′), and 3.33 (dd, 1H, H-2) ppm.

^{13}C NMR (125.76 MHz, D_2O): δ 99.6 (C-1′), 89.9 (C-1), 76.5, 76.2, 72.8, 72.7 (C-2, C-5′), 71.7 (C-2′), 69.3 (C-4′), and 60.5 (C-6, C-6′) ppm.

HRMS: calculated for $C_{12}H_{21}O_{10}N_3Na$, $[M + Na]^+$: 390.112 and measured: 390.110.

2-[2-(2-Azidoethoxy)ethoxy]ethyl O-(α-D-glucopyranosyl)-(1→4)-β-D-glucopyranoside (Mal-TEG-N$_3$). Peracetylated maltose (4.4 g, 6.4 mmol) was dissolved in dry CH_2Cl_2 (20 mL, under an argon atmosphere). 2-[2-(2-Chloroethoxy)ethoxy]ethanol (5 mL, 35 mmol, 5.5 equiv) was added to the solution, and the reaction mixture was cooled on an ice bath. $BF_3{\cdot}OEt_2$ (6.5 mL, 53 mmol, 8.3 equiv) was added dropwise, and the reaction mixture was slowly warmed to r.t. and left to stir for 5 h (MALDI-TOF analysis was utilized to monitor the reaction progress: $[M + Na]^+$ calculated for $C_{32}H_{47}ClO_{20}Na$: 809.22; observed: 809.65). The reaction mixture was cooled on an ice bath and neutralized with Et_3N. The mixture was brought to r.t., diluted with CH_2Cl_2 (30 mL), and washed with saturated $NaHCO_3$ solution (30 mL) and brine (30 mL). The organic phase was separated, dried over Na_2SO_4, filtered, and concentrated. The crude product was partially purified by column chromatography (EtOAc/hexane 2:1; R_f = 0.35 in EtOAc/hexane 1:1) to give an oil (4.6 g). The partially purified product was utilized as such in the following step.

The oil (4.6 g) was dissolved in dry DMF (30 mL), and Bu_4NI (2 g, 5.85 mmol, ∼1 equiv) and NaN_3 (2.3 g, 35 mmol, ∼6 equiv) were added. The resulting mixture was refluxed at 87 °C overnight (MALDI-TOF analysis was utilized to monitor the reaction progress; $[M + Na]^+$ calculated for $C_{32}H_{47}N_3O_{20}Na$: 816.26; observed: 816.47) and concentrated. The crude product was filtered through a pad of silica (EtOAc/hexane 3:1; R_f = 0.39 in EtOAc/hexane 3:1) (impurities still present). The partially purified product was utilized as such in the following step.

The crude product was dissolved in dry MeOH (10 mL), and the pH was adjusted to 10−11 with a 5 M solution of NaOMe. TLC-monitoring ($MeOH/CH_2Cl_2$ 1:3) of the reaction progress indicated that the reaction was complete after 1.5 h. The reaction mixture was neutralized with AG 50-X8 (H^+-form), diluted with MeOH (20 mL), filtered, and concentrated to give the crude product. The crude product was purified by column chromatography ($MeOH/CH_2Cl_2$ 1:3) to give the title compound as a white foam (870 mg, 1.7 mmol, yield over three steps: 27%). Analytical data was identical to the literature data.[32]

https://dx.doi.org/10.1021/acs.biomac.9b01596
Biomacromolecules 2020, 21, 955−965

Synthesis of PNVCL Nanogels. PNVCL nanogels were synthesized via precipitation polymerization according to a literature protocol.[16] The synthesis is presented in Figure 2. In a typical

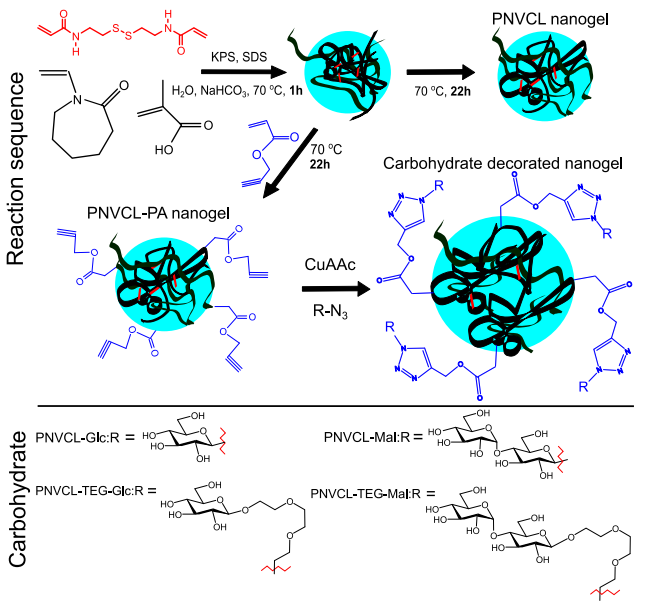

Figure 2. Synthesis of the PNVCL and PNVCL−PA nanogels and conjugation of carbohydrate azides to PNVCL−PA to yield carbohydrate-decorated nanogels: PNVCL−Glc, PNVCL−TEG−Glc, PNVCL−Mal, and PNVCL−TEG−Mal.

reaction, the monomers NVCL (1.880 g, 13.5 mmol), methacrylic acid (MAA, 20 mg, 0.23 mmol), the crosslinker BAC (20 mg, 0.077 mol), and the surfactant sodium dodecyl sulfate (SDS, 50 mg, 0.0173 mmol) together with a base $NaHCO_3$ (50 mg) were dissolved in 196 g of water. A rotation speed of 500 rpm was used. The reaction flask was flushed with nitrogen for 30 min at r.t., and then transferred to a preheated oil bath for 30 min until the reaction mixture was at 70 °C. The initiator, potassium persulfate (KPS 0.050 g), was dissolved in 4 g of water and flushed with N_2 gas for 20 min. The reaction was started by adding the KPS solution to the reaction flask. When propargyl acrylate (PA, 100 mg, 0.908 mmol) was used in the synthesis, it was added after 1 h of reaction time to yield the surface-functionalized particles. Overall, the reaction time was 23 h. The reaction mixture was purified via dialysis (MWCO 12−14 000 g/mol) against water. The dispersion was freeze-dried to obtain the dry product.

Conjugation of Carbohydrate Azides to Nanogels. Fifty milligrams of particles (22.7×10^{-6} mol PA according to feed) and 5 equiv of the corresponding carbohydrate azide (113.5×10^{-6} mol) were dissolved in 0.8 mL 0.1 M phosphate buffer (pH = 7.4) and nitrogen was bubbled through the solution for 1 h, and then the flask was placed in an ice bath. Copper acetate monohydrate (2.27×10^{-6} mol) and the carbohydrate ligand for copper (I) (2.27×10^{-6} mol) were dissolved in 0.1 mL water. Ascorbic acid, 11.4×10^{-6} mol, dissolved in 0.1 mL H_2O, was added to the particle solution under stirring. The reaction time was 48 h. Particles were purified via dialysis (MWCO 12−14 000 g/mol) against water. The dispersion was freeze-dried to obtain the dry product. The mass of the end product ranged from 45 to 55 mg, depending on the carbohydrate building block used.

Characterization. The NMR spectra were recorded using a Bruker Avance III NMR spectrometer (^{1}H: 500.13 MHz, ^{13}C: 125.76 MHz). The probe temperature during the experiments was kept at 23 °C. Chemical shifts were calibrated relative to the residual solvent signals.

Infrared spectra were recorded using a Perkin Elmer Spectrum One FT-IR spectrometer with ATR accessory. UV−vis spectra were recorded on a Shimadzu UV-1601PC spectrophotometer or with a Jasco V-750 spectrophotometer.

Mean hydrodynamic diameter (D_h) of the nanogels (0.25 g/L in 10 mM HEPES pH = 7.4) as a function of temperature was determined using a Malvern Zetasizer Nano ZS (laser wavelength: 633 nm, scattering angle: 173°). Measurements were performed from 16 to 79 °C at 3 °C intervals equilibrating 15 min at every measured point. Samples were equilibrated in a fridge overnight and filtered with a 1 μm glass fiber syringe filter before the measurement.

Hydrodynamic diameter distributions were obtained with CONTIN from measurements at 25 °C at 90° angle using a setup consisting of a Brookhaven instrument BI-200SM goniometer, BICTurboCorr digital pseudo-cross-correlator, and a BI-CrossCorr detector including two BIC-DS1 detectors. The pseudo-cross-correlation functions were collected in a self-beating method, and the used light source was a Coherent Sapphire 488 nm blue laser with incident light set between 10 and 30 mW. The sample cell temperature was controlled with a Lauda RC 6 CP thermostat.

Multiangle measurements for selected samples were performed at 25 °C with the same instrument used for the hydrodynamic radius distribution measurements. The detection angles were 130, 90, 70, 50, and 30°. Dynamic light scattering measurements at the respective angles were used to obtain the hydrodynamic radius using cumulant and CONTIN methods. Averages of the respective values are given in Table 2. The angular dependence of the scattered light was also used to obtain the radius of gyration for the samples. More details are presented in the Results and Discussion section.

The carbohydrate−lectin interactions were studied via a precipitation assay. Six microliters of 50 mg/mL nanogel dispersion in water were added per 1 mL of con A solution, and the particles were let to aggregate for 30 min, after which they were removed from dispersion via centrifugation for 20 min at 10 000 rpm, 9391 rcf. The supernatant was weighted, and its lectin concentration was determined from UV absorbance before the next nanogel addition.

Salt-induced aggregation was tested at 50 °C with 1 mg/mL aqueous nanogel samples. Two microliters of 2 M aqueous NaCl was added per 1 mL of nanogel dispersion. After a 15 min stabilization, the transmittance was measured, and then the next aliquot of saline water was added. Transmittance at 650 nm was plotted against salt concentration to find the aggregation and precipitation concentrations. The aggregation point was the NaCl concentration, where the transmittance discontinuously decreased. The precipitation point was determined as the concentration where visible precipitation transpired or where the transmittance had increased compared to the previous addition.

The fluorescence measurements were conducted with a Horiba Jobin Yvon Fluoromax-4 spectrofluorometer. Quartz cuvettes with 10 mm path length were used. Two microliters of a 10 mM aqueous ammonium salt of 8-anilino-1-naphthalenesulfonic acid (ANS) solution was added to a 2 mL 0.25 m/mL nanogel dispersion and mixed overnight. Emission spectra were measured at different temperatures ranging from 16 to 73 °C in 3° intervals, after 15 min of stabilization at each temperature with 379 nm excitation wavelength and using 3.3 nm excitation and 2 nm emission slits.

RESULTS AND DISCUSSION

Synthesis and Characterization of PNVCL and PNVCL−PA Nanogels. The PNVCL and PNVCL−PA nanogels were synthesized via precipitation polymerization. SDS was used in the synthesis and removed afterward by dialysis. The toxicity of the surfactant remaining in the gel particles has been studied elsewhere.[7] The PNVCL−PA gels containing propargyl groups were prepared by a semibatch technique in which the PA comonomer was added 1 h after the start of the reaction. This will generate particles with the propargyl groups located on the surface. At that instant, approximately 85% of the final monomer (NVCL) conversion

https://dx.doi.org/10.1021/acs.biomac.9b01596
Biomacromolecules 2020, 21, 955−965

had been reached (see the Supporting Information, Figures S9 and S10).

The ^{1}H NMR spectra of PVCL and PVCL−PA nanogels in D_2O (Figure 3) are similar, and the chemical shifts arising from

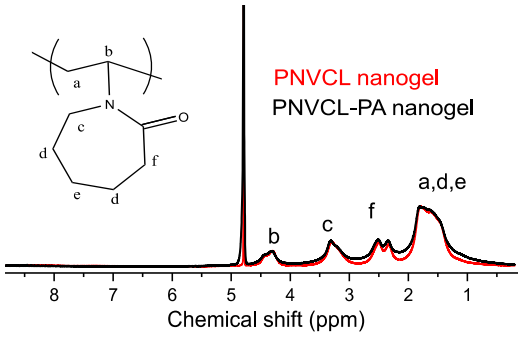

Figure 3. ^{1}H NMR spectra of the PNVCL and PNVCL−PA nanogels.

PA are not distinguishable. This is not surprising when the amount (6.7 mol % in feed with respect to NVCL) and poor aqueous solubility of PA are taken into account. In addition, the signals from PA and PNVCL are overlapping in the spectrum (^{1}H NMR spectra of PA in D_2O is shown in the Supporting Information, Figure S11).

The IR spectra of PNVCL and PNVCL−PA are displayed in Figure 4. All of the characteristic peaks of PNVCL can be

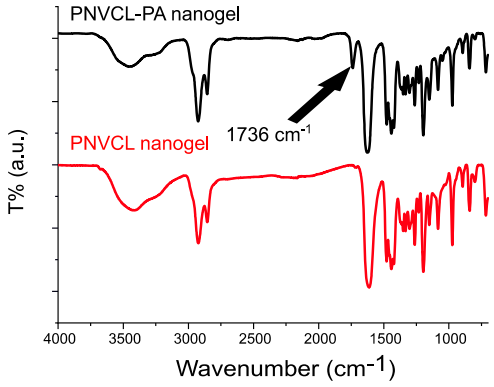

Figure 4. IR spectra of PNVCL and PNVCL−PA nanogels. The band indicating the incorporation of PA to the nanogels is marked with an arrow.

identified in both spectra.[36] Additionally, a band at 1736 cm^{-1} is seen in the spectrum of the PNVCL−PA nanogel. This band originates from the carbonyl of the acrylate group in PA and confirms the successful incorporation of PA in the product.

Functionalization of the PNVCL−PA Nanogel with Carbohydrate Azides. The azido-glucosides and maltosides (compounds in Figure 1) were conjugated to the nanogels by a CuAAC reaction featuring a Cu(I)-ligand[35] and in high yields. The carbohydrate-coated nanogels will, from this stage onwards, be referred to as PNVCL−Glc, PNVCL−TEG−Glc, PNVCL−Mal, and PNVCL−TEG−Mal (named based on the used carbohydrate, see Figure 2). The IR spectra of the carbohydrate azides, PVCL−PA, and the carbohydrate-coated nanogels are shown in Figure 5. The most intense bands in the spectra of the carbohydrate monomers are the C−O at 1045 cm^{-1} and the azide at 2095 cm^{-1}.[37,38] In the spectra of the functionalized nanogels, a peak from the carbohydrate C−O

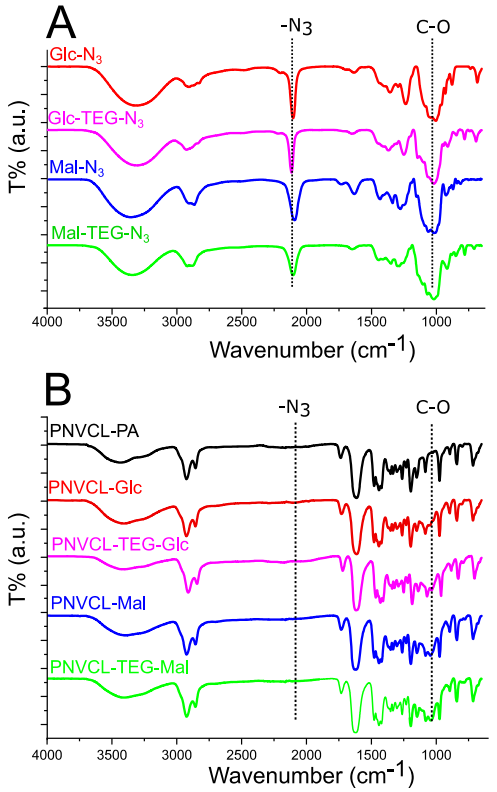

Figure 5. IR spectra of (A) the carbohydrate azides and (B) the PNVCL−PA and carbohydrate-coated PNVCL nanogels.

can be identified, and the azide band is absent, thus indicating the successful conjugation of the carbohydrates to the nanogel backbones.

The successful incorporation of the carbohydrates is clear from the appearance of the triazole-proton in the ^{1}H NMR spectra (see Figure 6). The ^{1}H NMR spectra of the other

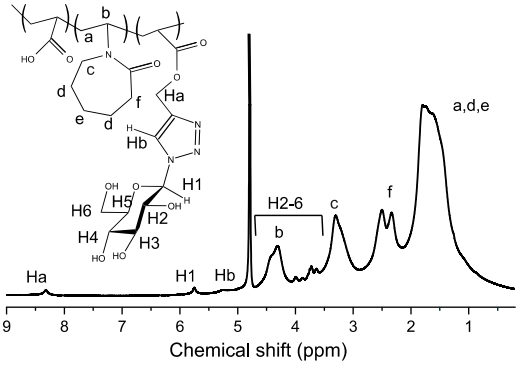

Figure 6. ^{1}H NMR spectra of PNVCL−Glc nanogel.

carbohydrate-decorated particles are presented in the Supporting Information, Figures S13−S15. On a general level, the signals from the triazole ring and from adjacent −CH_2− (8.3 and 5.2 ppm) can be identified in all of the carbohydrate-decorated PNVCL nanogels. Integrals of the peaks were used to determine the amount of incorporated carbohydrates in the nanogels (summary listed in Table 1). All of the nanogels contained approximately 4 mol % of carbohydrates when referenced to the NVCL units. The reason for these observations can be contributed to the long reaction times

https://dx.doi.org/10.1021/acs.biomac.9b01596
Biomacromolecules 2020, 21, 955−965

Table 1. Integrated NMR-Values and mol % of Incorporated Carbohydrates

product	∫(8.3 ppm)	∫(5.2 ppm)	mol % carbohydrate
PNVCL−PA	0	0	0
PNVCL−Glc	0.038	0.081	3.9
PNVCL−TEG−Glc	0.037	0.075	3.7
PNVCL−Mal	0.034	0.084	3.9
PNVCL−TEG−Mal	0.041	0.088	4.3

(48 h) and the excess of azides used, which drives the reaction to completion. The kinetics of one of the conjugation reactions was followed by ^{1}H NMR spectroscopy, and the reaction was essentially complete in 8 h (see the Supporting Information, Figure S16).

Size and Thermal Response of the Nanogels. Dynamic light scattering was employed to study the sizes and size distributions of the nanogels in aqueous buffer (10 mM HEPES, pH = 7.4). The size distributions of PNVCL and PNVCL−PA nanogels at 25 °C, measured at 90° are shown in Figure 7. The addition of PA does not change the average size

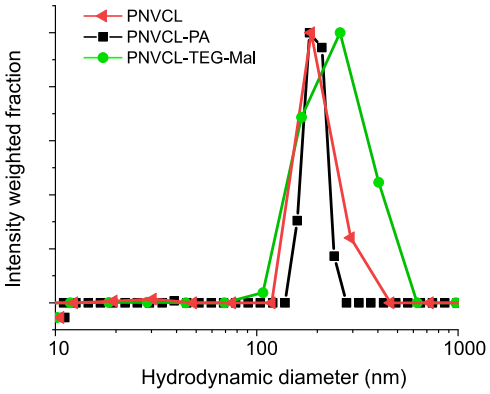

Figure 7. Size distribution of PNVCL, PNVCL−PA, and PNVCL−TEG−Mal nanogels.

of the nanogels, but the size distribution narrows. Attaching carbohydrates, on the other hand, leads to an increase in the average size and affects the size distribution (see Figures 7 and S18). The angular dependence of the scattered light intensity can be used to analyze the morphology of the scattering particles, including the radius of gyration (R_g).[39,40] Multiangle light scattering measurements were performed on the following samples: PNVCL, PNVCL−PA, and PNVCL−TEG−Mal, and the results are presented in Table 2 and Figure 8.

In Table 2, the hydrodynamic size differences are clear; PNVCL−PA and PNVCL nanogels have a similar hydrodynamic radius, but PNVCL has a higher dispersity. Of the three nanogels, the PNVCL−TEG−Mal particles were the largest and showed the highest dispersity. Here, the angular dependence was analyzed by comparing suitable models, which

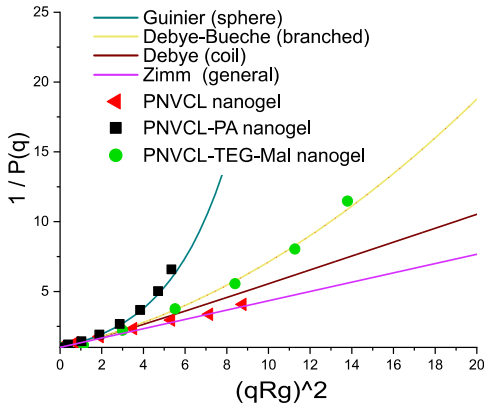

Figure 8. Inversed particle structure factor [P_q is a function of normalized scattering intensity, $P(q) \equiv I(q)/I\,(q = 0)$] plotted against a squared scattering vector ($q = (4\pi n_o/\lambda)\sin\theta/2$) times squared radius of gyration (R_g). Solid lines represent theoretical curves for selected geometries of scatterers.

have been derived for different geometries; Debye−Bueche (for branched objects), Zimm (a general model), or Guinier (for draining spheres) to find the best fit between theory/model and the experimental data. R_g was obtained from the initial slope of the function.[39,40] In Table 2, differences in morphologies are reflected in the R_g/R_h ratio, as well as in the model that gave the best fit in each case. A graphical presentation of the angular dependencies is presented in Figure 8, where the functions from different models are drawn as continuous lines. From this presentation of the data, the difference between the nanogels is evident. PNVCL−PA is more compact than PNVCL−TEG−Mal, whereas PNVCL−TEG−Mal is more compact than the PNVCL nanogel.

The more compact structure of PNVCL−PA compared to PNVCL nanogel, evidenced by light scattering, is due to either the solvophobic nature of PA (hydrophobic interaction) or due to additional chemical crosslinking. The alkyne functionality of PA is known to react via a free radical polymerization mechanism, even though the reactivity of the alkyne is but a fraction of the reactivity of the alkane in PA.[41] The more compact structure of carbohydrate-decorated PNVCL nanogels supports the hypothesis that a part of the PA triple bonds has reacted during the polymerization and formed crosslinks.

The differences in the structural features of the nanogels affect their thermal behavior, as seen in Figure 9. The most open of the nanogels, the PNVCL nanogel, forms large intermolecular aggregates upon heating as the PNVCL chains become insoluble. This type of behavior is typical for linear PNVCL and for slightly crosslinked PNVCL nanogels.[29,42,43] More compact nanogels on the other hand, tend to shrink upon heating but do not necessarily aggregate.[7,10−13] The gel collapse is called volume phase transition (VPT). Both the PNVCL−PA and PNVCL−TEG−Mal nanogels exhibit VPT.

Table 2. Analysis from Multiangle Light Scattering Studies[a]

nanogel	R_h*	Poly.*	R_h**	R_g	R_g/R_h**	model used to calculate R_g
PNVCL	101	0.12	105	95	0.94	Zimm
PNVCL−PA	96	0.08	98	70	0.71	Guinier
PNVCL−TEG−Mal	129	0.16	133	119	0.89	Debye−Bueche

[a] R_h* based on cumulant analysis, Poly*. is a dispersity estimation based on the 2nd cumulant fit, R_h** is from CONTIN. Values for R_h*, Poly*, and R_h** are averages over multiple angles.

https://dx.doi.org/10.1021/acs.biomac.9b01596
Biomacromolecules 2020, 21, 955−965

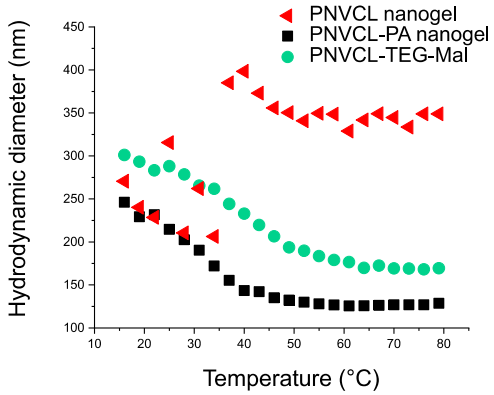

Figure 9. Mean diameter (nm) of PNVCL and PVNCL−PA nanogels in aqueous buffer (10 mM HEPES, pH = 7.4) as a function of temperature.

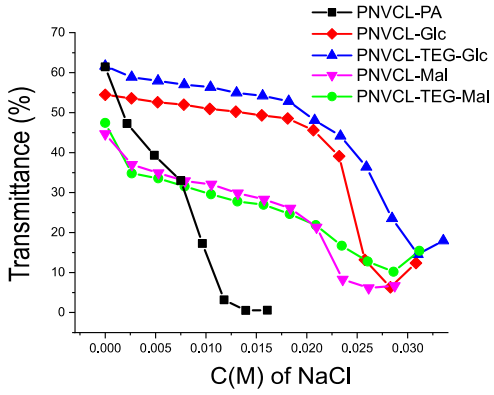

Figure 10. Stability of selected nanogels against NaCl additions at 50 °C; transmittance at 650 nm plotted against salt concentration.

The diameter of PNVCL−PA decreased from 230 nm at 22 °C to 130 nm at 70 °C and that of PNVCL−TEG−Mal from 280 nm at 22 °C to 170 nm at 70 °C. The other carbohydrate-coated PNVCLs also shrank upon heating (the results are presented in the Supporting Information, Figure S19). All of the carbohydrate-containing nanogels are larger compared to the PNVCL−PA at all temperatures. It appears that the increase in hydrophilic character (from the carbohydrates) would be accompanied by a shift of the volume phase transition to higher temperatures. The temperature where half of the overall shrinkage has occurred (VPT midpoint) is 31 °C for PNVCL−PA, 34 °C for PNVCL−Glc, 37 °C for both PNVCL−TEG−Glc and PNVCL−Mal, and 40 °C for PNVCL−TEG−mal. These results follow a logical trend, and it is clear that both the carbohydrate and the spacer contribute to the properties (in roughly equal proportions). This is important to note, especially when designing carbohydrate-containing nanogels for biomedical applications since their properties can be fine-tuned by selecting an appropriate chemical spacer. A broader series of spacers would nevertheless need to be screened to obtain a more complete picture, but the triethylene glycol spacer seems to have a similar effect as a carbohydrate residue.

Colloidal Stability. The PVCL−PA and PNVCL−carbohydrate nanogels are colloidally stable in water and aqueous buffer (10 mM HEPES, pH = 7.4) upon heating up to at least 70 °C as seen in Figure 9. The nanogels, however, precipitate above their VPTT upon the addition of salt. This is one of the key factors when considering the applicability of material in physiological conditions or in biomedical applications with the medium being warm and having a high ionic strength. The solubility of PNVCL is known to be sensitive to ionic strength as well as to the type of ions.[44−48] Thus, the colloidal stability of the present particles was investigated with salting-out tests. To compare the tolerance of the nanogels against salt addition, 1 mg/mL dispersions of the nanogels were titrated with 2 M NaCl at 50 °C (see Figure 10). From the figure, it can be seen how transmittance decreased as the solvent quality changed upon the addition of NaCl. The steepest parts of the curves were identified to correspond to aggregation. The size distributions obtained with DLS for PNVCL−PA at selected NaCl concentrations are presented in the Supporting Information, Figure S21. The endpoints of the curves are the precipitation concentrations. At this point, the aggregates started effectively to sediment to the bottom of the vial, which is why the transmittance is slightly higher compared to the transmittance at a lower NaCl concentration. As can be seen, the carbohydrate-decorated PNVCL-particles are more stable than the parent PNVCL−PA nanogel. There are both obvious and more subtle differences between the attached carbohydrate moieties. The underlying reasons are, however, not easily explained. The maltoside-containing nanogels are, surprisingly, less stable than the corresponding glucosides, although they contain an increased amount of hydroxyl groups, which should be advantageous in maintaining the stability in ionic solutions. A broader series of derivatives would be needed to shed more light on these observations and uncover the molecular basis. Regardless, the triethylene glycol spacer has a subtle stabilizing effect, which is noticeable in both the glucose and maltose series. Based on this limited set of conjugates, it is clear that the colloidal properties can be fine-tuned, to a certain extent, by selecting appropriate spacers and carbohydrates. The carbohydrates used to coat the surfaces in the current study do not prevent the aggregation of the nanogels, a 35 mM concentration of NaCl is enough to precipitate all of the nanogels.

Lectin Binding. To uncover whether the carbohydrates residing on the surface of the PVCL-nanogels could interact with other biomolecules in a biological context, a preliminary lectin assay with Con A was conducted. The precipitation studies were performed by the addition of Con A solutions to small aliquots of the nanogel dispersions. When Con A binds to the nanogels, it causes them to precipitate and they can then be removed from the dispersions by centrifugation. The amount of Con A remaining in the dispersions can afterward be determined based on the UV absorbance at 278 nm. The results from these studies are presented in Figure 11.

The alkyne-functionalized PVCL−PA did not have an affinity toward Con A as expected (see Figure 11). The carbohydrate-coated nanogels bound to Con A in the increasing order PVCL−Glc−TEG < PVCL−Glc < PVCL−Mal < PVCL−Mal−TEG. The differences in binding of Con A to the different carbohydrate nanogels are rationalized as follows. Con A is known to have an affinity toward the α-D-glucopyranosyl and α-D-mannopyranosyl residues.[49,50] Maltose contains a terminal α-D-glucopyranosyl residue, and the PNVCL−Mal/PNVCL−TEG−Mal particles were therefore expected to bind to Con A. Our studies confirmed that the interaction of these particles with Con A is indeed strong (see Figure 11). There is a subtle difference between the interaction of the PNVCL−Mal and PNVCL−TEG−Mal particles with

https://dx.doi.org/10.1021/acs.biomac.9b01596
Biomacromolecules 2020, 21, 955−965

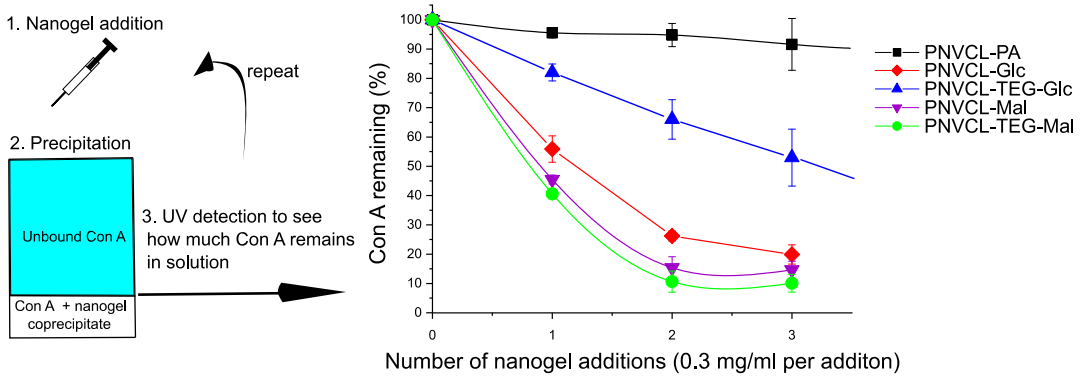

Figure 11. Con A precipitation assay. For details, see the Experimental Section. The data points are averages of two measurements, and the standard deviation is presented as error margins.

Con A. This may be attributed to the more flexible spacer in the TEG−Mal-derivative although it should be pointed out that the difference is insignificant.

The glucose derivatives (PNVCL−Glc and PNVCL−TEG−Glc), on the other hand, contain a β-D-glucopyranosyl unit for which Con A is known to have a lower affinity. This is clear from the PNVCL−TEG−Glc nanogel as the binding to Con A is significantly lower than for the maltose containing derivatives. However, the PNVCL−Glc particles bind to Con A in a manner similar to the maltose containing particles. The only difference between the PNVCL−TEG−Glc and PNVCL−Glc is the spacer, and therefore the observed interactions can be attributed to the triazole ring, which is spatially close to the glucopyranosyl residue in the PNVCL−Glc particles. In other words, in the case of the PNVCL−Glc particles, the lectin interaction is pronouncedly affected by the spacer as it is in close proximity to the carbohydrate recognition domain during the recognition process, i.e., the triazole ring may therefore affect the binding process to a high degree. Maltose is a disaccharide, and thus, there is one sugar residue between the spacer and the recognized sugar unit. This is why in the maltose case, the effect of the spacer is lower. While we tried to supplement the binding study with the use of isothermal calorimetry (ITC) to quantify binding, our preliminary tests failed because the PNVCL−carbohydrate nanogels precipitated upon contact with Con A.

To investigate, if the temperature could be used to switch the binding mode of the carbohydrates, the Con A binding studies were performed at both room temperature and 37 °C with PNVCL−TEG−Mal (Figure 12). Surprisingly, temperature dependence could not be observed although the PNVCL−TEG−Mal exists in a swollen state at room temperature and in a partially collapsed state at 37 °C, which is close to the VPT midpoint. Intuitively, we had assumed that the binding would be stronger at a higher temperature owing to the enrichment of the maltose on the particle surface during gel collapse. In fact, this is what has been observed with PNIPAM-based microgels with mannose units randomly copolymerized on the polymer.[30,31] The fact that the PNVL−TEG−Mal binding to Con A did not display a thermoresponsive behavior of this kind confirms that the maltose residues are located on the surface of the nanogels independent of the surrounding temperature and available for interactions with biomolecules. Due to the selected synthetic route, the particles have interacting surface functions and a thermoresponsive inner structure.

Interactions of Nanogels with a Fluorescent Probe. Because experimental evidence up to this point indicated that the surface modification also affects the internal structure of the nanogels, an attempt was made to examine the structural differences with the fluorescent probe 8-anilino-1-naphthalenesulfonate (ANS). ANS is a probe, which in water exhibits practically no fluorescence but turns fluorescent upon contact with a polymer or a membrane.[51] We have earlier used ANS in studies on neat and AuNP-decorated PNVCL nanogels.[16]

The intensities of fluorescence emission from three samples are plotted as functions of temperature in Figure 13. ANS in the PNVCL−PA nanogels emits strongly already at temperatures below ambient. It is known that in aqueous solutions of linear PNVCL, hydrophobic pockets (partly folded regimes)

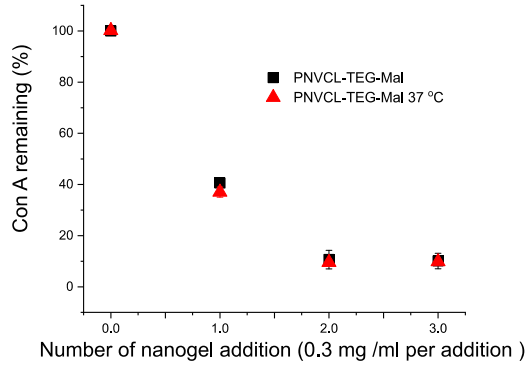

Figure 12. Precipitation assay of Con A with PNVCL−TEG−Mal nanogel at room temperature and 37 °C.

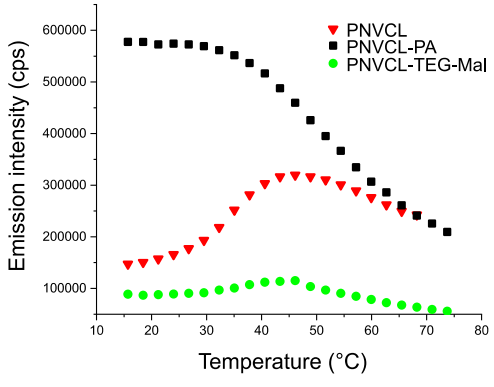

Figure 13. Fluorescence emission from ANS in nanogel dispersions.

https://dx.doi.org/10.1021/acs.biomac.9b01596
Biomacromolecules 2020, 21, 955−965

exist inside the coil even at room temperature[47,52] and that their number is elevated in PNVCL gel particles.[16] Upon heating, the emission intensity from PNVCL−PA nanogel decreased, indicating the diffusion of the probe out from the particles. This was not due to the precipitation of the nanogels, and therefore it was attributed to gel collapse.

The PNVCL nanogels behaved differently because of their more open structure. The emission intensity was, e.g., considerably lower than that of PNVCL−PA at low temperatures. During the thermal transition, the intensity from the PNVCL sample first increased and then decreased. The experiments proved that hydrophobic pockets existed already at low temperatures and increased in number at higher temperatures. Importantly, the hydrophobic modification of the surface was accompanied by an increased abundance of hydrophobic pockets in the case of PNVCL−PA. At elevated temperatures, the probe diffused partly out from the PNVCL nanogels, in a manner similar to PNVCL−PA.

The carbohydrate-decorated nanogel PNVCL−TEG−Mal is more hydrophilic and solvated in the studied temperature range. It differs from the PNVCL−PA and PNVCL nanogels, which confirms that the carbohydrate moieties affect the structural properties of the entire nanogel. Based on the emission spectra, the amount of hydrophobic pockets is significantly decreased in the PNVCL−TEG−Mal nanogel compared to the parent PNVCL−PA nanogel and also in comparison to the PNVCL nanogels. However, the behavior otherwise has characteristics between that of PNVCL and PNVCL, i.e., ANS is first absorbed to the collapsed particle during the volume phase transition and then expelled from the nanogels. The low emission intensity within the whole temperature range reveals the very soft and swollen structure of the PNVCL−TEG−Mal nanogel.

CONCLUSIONS

Thermoresponsive PNVCL-based nanogels were synthesized in a semibatch precipitation polymerization. Propargyl acrylate, PA, was used as a comonomer to introduce terminal alkyne groups on the gel surfaces. The PNVCL−PA particles had a more narrow hydrodynamic size distribution and were more compact than the parent PNVCL molecule. The terminal alkyne was modified with four different azido-glucosides and maltosides via a CuAAC reaction in high yields. The carbohydrate-decorated PNVCL nanogels contained 4 mol % of the carbohydrates. Carbohydrate-decorated PNVCL nanogels have potential as drug delivery systems. The nanogels are relatively large but are soft and deformable. Various aspects of our model nanogels containing either an attached monosaccharide or disaccharide with two separate linkers were thoroughly studied. The nanogels shrank in aqueous buffer (10 mM HEPES, pH = 7.4) during heating and the addition of salt-induced aggregation and precipitation of the nanogels at elevated temperature (measured at 50 °C). The carbohydrate-decorated nanogels were more stable against salt-induced aggregation, and the TEG-spacer was found to have a subtle effect. To address the availability of the carbohydrates toward other biomolecules, which would be present in a biological context, a preliminary binding study with Con A was included. The maltose derivatives bound stronger to Con A than the glucose derivatives as expected; however, PNVCL−Glc had a surprisingly strong binding, which was herein considered to be due to the spatial location of the triazole moiety. The recognition of the carbohydrates by Con A was equally efficient below and in the middle of the volume phase transition temperature. This indicates that the carbohydrates are located on the surface of the nanogels, both in swollen and partially collapsed states. The structural features of the nanogels were further studied by light scattering and fluorescence. The data revealed that the carbohydrate-decorated PNVCL nanogels are more swollen and hydrophilic than the unconjugated PNVCL-particles at all measured temperatures. Taken together, the results of our work show that the modification of nanogels by carbohydrates affects the properties of the gels on the whole. Furthermore, it is clear that the structural features and properties of the end products can be fine-tuned by alternating the carbohydrate structures and spacers used. A broader library of carbohydrates and spacers are needed to shed more light on these relationships to gain insights into the appropriate constructs for biomedical purposes.

ASSOCIATED CONTENT

Supporting Information

The Supporting Information is available free of charge at https://pubs.acs.org/doi/10.1021/acs.biomac.9b01596.

NMR spectra of the synthesized carbohydrate azides, glucose, and maltose-functionalized nanogels; kinetics of nanogel synthesis and functionalization reaction; light scattering data of glucose- and maltose-functionalized nanogels (PDF)

AUTHOR INFORMATION

Corresponding Author

Heikki Tenhu − *Department of Chemistry, University of Helsinki, Helsinki 00014, Finland;* orcid.org/0000-0001-5957-4541; Email: heikki.tenhu@helsinki.fi

Other Authors

Joonas Siirilä − *Department of Chemistry, University of Helsinki, Helsinki 00014, Finland*

Sami Hietala − *Department of Chemistry, University of Helsinki, Helsinki 00014, Finland;* orcid.org/0000-0003-1448-1813

Filip S. Ekholm − *Department of Chemistry, University of Helsinki, Helsinki 00014, Finland;* orcid.org/0000-0002-4461-2215

Complete contact information is available at: https://pubs.acs.org/10.1021/acs.biomac.9b01596

Notes

The authors declare no competing financial interest.

ACKNOWLEDGMENTS

Jane and Aatos Erkko Foundation, University of Helsinki research funds, and Academy of Finland are acknowledged for funding the research.

REFERENCES

(1) Plamper, F. A.; Richtering, W. Functional Microgels and Microgel Systems. *Acc. Chem. Res.* **2017**, *50*, 131−140.

(2) Agrawal, G.; Agrawal, R. Functional Microgels: Recent Advances in Their Biomedical Applications. *Small* **2018**, *14*, No. 1801724.

(3) Karg, M.; Pich, A.; Hellweg, T.; Hoare, T.; Lyon, L. A.; Crassous, J. J.; Suzuki, D.; Gumerov, R. A.; Schneider, S.; Potemkin, I. I.; Richtering, W. Nanogels and Microgels: From Model Colloids to Applications, Recent Developments, and Future Trends. *Langmuir* **2019**, *35*, 6231−6255.

(4) Yang, D.; Viitasuo, M.; Pooch, F.; Tenhu, H.; Hietala, S. Poly(N-acryloylglycinamide) microgels as nanocatalyst platform. *Polym. Chem.* **2018**, *9*, 517−524.
(5) Zhang, Y.; Zhang, H.; Liu, P.; Sun, H.; Li, B.; Wang, W. Programming Hydrogen Production via Controllable Emulsification/Demulsification in a Switchable Oil−Water System. *ACS Sustainable Chem. Eng.* **2019**, *7*, 7768−7776.
(6) Liu, J.; Detrembleur, C.; Debuigne, A.; De Pauw-Gillet, M.; Mornet, S.; Vander Elst, L.; Laurent, S.; Duguet, E.; Jérôme, C. Glucose-, pH- and thermo-responsive nanogels crosslinked by functional superparamagnetic maghemite nanoparticles as innovative drug delivery systems. *J. Mater. Chem. B* **2014**, *2*, 1009.
(7) Wang, Y.; Nie, J.; Chang, B.; Sun, Y.; Yang, W. Poly(vinylcaprolactam)-Based Biodegradable Multiresponsive Microgels for Drug Delivery. *Biomacromolecules* **2013**, *14*, 3034−3046.
(8) Cortez-Lemus, N. A.; Licea-Claverie, A. Poly(N-vinylcaprolactam), a comprehensive review on a thermoresponsive polymer becoming popular. *Prog. Polym. Sci.* **2016**, *53*, 1−51.
(9) Macchione, M. A.; Guerrero-Beltrán, C.; Rosso, A. P.; Euti, E. M.; Martinelli, M.; Strumia, M. C.; Muñoz-Fernández, M. Á. Poly(N-vinylcaprolactam) Nanogels with Antiviral Behavior against HIV-1 Infection. *Sci. Rep.* **2019**, *9*, No. 5732.
(10) González-Ayón, M. A.; Sañudo-Barajas, J. A.; Picos-Corrales, L. A.; Licea-Claverie, A. PNVCL-PEGMA nanohydrogels with tailored transition temperature for controlled delivery of 5-fluorouracil. *J. Polym. Sci., Part A: Polym. Chem.* **2015**, *53*, 2662−2672.
(11) Lou, S.; Gao, S.; Wang, W.; Zhang, M.; Zhang, Q.; Wang, C.; Li, C.; Kong, D. Temperature/pH dual responsive microgels of crosslinked poly(N-vinylcaprolactam-co-undecenoic acid) as biocompatible materials for controlled release of doxorubicin. *J. Appl. Polym. Sci.* **2014**, *131*, No. 41146.
(12) Madhusudana Rao, K.; Mallikarjuna, B.; Krishna Rao, K. S. V.; Siraj, S.; Chowdoji Rao, K.; Subha, M. C. S. Novel thermo/pH sensitive nanogels composed from poly(N-vinylcaprolactam) for controlled release of an anticancer drug. *Colloids Surf., B* **2013**, *102*, 891−897.
(13) Vihola, H.; Laukkanen, A.; Tenhu, H.; Hirvonen, J. Drug release characteristics of physically cross-linked thermosensitive poly(N-vinylcaprolactam) hydrogel particles. *J. Pharm. Sci.* **2008**, *97*, 4783−4793.
(14) Richtering, W.; Pich, A. The special behaviours of responsive core-shell nanogels. *Soft Matter* **2012**, *8*, 11423−11430.
(15) Gau, E.; Mate, D. M.; Zou, Z.; Oppermann, A.; Töpel, A.; Jakob, F.; Wöll, D.; Schwaneberg, U.; Pich, A. Sortase-Mediated Surface Functionalization of Stimuli-Responsive Microgels. *Biomacromolecules* **2017**, *18*, 2789−2798.
(16) Siirilä, J.; Karesoja, M.; Pulkkinen, P.; Malho, J.; Tenhu, H. Soft poly(N-vinylcaprolactam) nanogels surface-decorated with AuNPs. Response to temperature, light, and RF-field. *Eur. Polym. J.* **2019**, *115*, 59−69.
(17) Kolb, H. C.; Finn, M. G.; Sharpless, K. B. Click Chemistry: Diverse Chemical Function from a Few Good Reactions. *Angew. Chem., Int. Ed.* **2001**, *40*, 2004−2021.
(18) Lowe, A. B.; Hoyle, C. E.; Bowman, C. N. Thiol-yne click chemistry: A powerful and versatile methodology for materials synthesis. *J. Mater. Chem.* **2010**, *20*, 4745−4750.
(19) de Castro, C. E.; Ribeiro, C. A. S.; da Silva Maria, C. C.; Dal-Bó, A. G.; Giacomelli, F. C. Sweetness Reduces Cytotoxicity and Enables Faster Cellular Uptake of Sub-30 nm Amphiphilic Nanoparticles. *Langmuir* **2019**, *35*, 8060−8067.
(20) Miura, Y.; Hoshino, Y.; Seto, H. Glycopolymer Nanobiotechnology. *Chem. Rev.* **2016**, *116*, 1673−1692.
(21) Ahmed, M.; Wattanaarsakit, P.; Narain, R. Cationic glyconanogels for epidermal growth factor receptor (EGFR) specific siRNA delivery in ovarian cancer cells. *Polym. Chem.* **2013**, *4*, 3829−3836.
(22) Burek, M.; Waśkiewicz, S.; Lalik, A.; Student, S.; Bieg, T.; Wandzik, I. Thermoresponsive microgels containing trehalose as soft matrices for 3D cell culture. *Biomater. Sci.* **2017**, *5*, 234−246.
(23) Gau, E.; Flecken, F.; Belthle, T.; Ambarwati, M.; Loos, K.; Pich, A. Amylose-Coated Biohybrid Microgels by Phosphorylase-Catalyzed Grafting-From Polymerization. *Macromol. Rapid Commun.* **2019**, *40*, No. 1900144.
(24) How, S.; Chen, Y.; Hsieh, P.; Wang, S.-S.; Jan, J. Cell-targeted, dual reduction- and pH-responsive saccharide/lipoic acid-modified poly(L-lysine) and poly(acrylic acid) polyionic complex nanogels for drug delivery. *Colloids Surf., B* **2017**, *153*, 244−252.
(25) Jans, A.; Rosencrantz, R. R.; Mandić, A. D.; Anwar, N.; Boesveld, S.; Trautwein, C.; Moeller, M.; Sellge, G.; Elling, L.; Kuehne, A. J. C. Glycan-Functionalized Microgels for Scavenging and Specific Binding of Lectins. *Biomacromolecules* **2017**, *18*, 1460−1465.
(26) Leite, D. C.; Kakorin, S.; Hertle, Y.; Hellweg, T.; da Silveira, N. P. Smart Starch−Poly(N-isopropylacrylamide) Hybrid Microgels: Synthesis, Structure, and Swelling Behavior. *Langmuir* **2018**, *34*, 10943−10954.
(27) Narain, R.; Wang, Y.; Ahmed, M.; Lai, B. F. L.; Kizhakkedathu, J. N. Blood Components Interactions to Ionic and Nonionic Glyconanogels. *Biomacromolecules* **2015**, *16*, 2990−2997.
(28) Tang, J. S. J.; Rosencrantz, S.; Tepper, L.; Chea, S.; Klöpzig, S.; Krüger-Genge, A.; Storsberg, J.; Rosencrantz, R. R. Functional Glyco-Nanogels for Multivalent Interaction with Lectins. *Molecules* **2019**, *24*, No. 1865.
(29) Aguirre, G.; Ramos, J.; Forcada, J. Synthesis of new enzymatically degradable thermo-responsive nanogels. *Soft Matter* **2013**, *9*, 261−270.
(30) Hoshino, Y.; Nakamoto, M.; Miura, Y. Control of Protein-Binding Kinetics on Synthetic Polymer Nanoparticles by Tuning Flexibility and Inducing Conformation Changes of Polymer Chains. *J. Am. Chem. Soc.* **2012**, *134*, 15209−15212.
(31) Paul, T. J.; Rübel, S.; Hildebrandt, M.; Strzelczyk, A. K.; Spormann, C.; Lindhorst, T. K.; Schmidt, S. Thermosensitive Display of Carbohydrate Ligands on Microgels for Switchable Binding of Proteins and Bacteria. *ACS Appl. Mater. Interfaces* **2019**, *11*, 26674−26683.
(32) Rahkila, J.; Ekholm, F. S.; Ardá, A.; Delgado, S.; Savolainen, J.; Jiménez-Barbero, J.; Leino, R. Novel Dextran-Supported Biological Probes Decorated with Disaccharide Entities for Investigating the Carbohydrate−Protein Interactions of Gal-3. *ChemBioChem* **2019**, *20*, 203−209.
(33) Díaz-Alvarez, L.; Ortega, E. The Many Roles of Galectin-3, a Multifaceted Molecule, in Innate Immune Responses against Pathogens. *Mediators Inflammation* **2017**, *2017*, No. 9247574.
(34) Emilitri, E.; Ranucci, E.; Ferruti, P. New poly(amidoamine)s containing disulfide linkages in their main chain. *J. Polym. Sci., Part A: Polym. Chem.* **2005**, *43*, 1404−1416.
(35) Ekholm, F. S.; Pynnönen, H.; Vilkman, A.; Koponen, J.; Helin, J.; Satomaa, T. Synthesis of the copper chelator TGTA and evaluation of its ability to protect biomolecules from copper induced degradation during copper catalyzed azide−alkyne bioconjugation reactions. *Org. Biomol. Chem.* **2016**, *14*, 849−852.
(36) Kozanoğlu, S.; Özdemir, T.; Usanmaz, A. Polymerization of N-Vinylcaprolactam and Characterization of Poly(N-Vinylcaprolactam). *J. Macromol. Sci., Part A: Pure Appl. Chem.* **2011**, *48*, 467−477.
(37) Ibrahim, M.; Alaam, M.; El-Haes, H.; Jalbout, A. F.; de Leon, A. Analysis of the structure and vibrational spectra of glucose and fructose. *Ecletica Quím.* **2006**, *31*, 15−21.
(38) Lieber, E.; Rao, C. N. R.; Chao, T. S.; Hoffman, C. W. W. Infrared Spectra of Organic Azides. *Anal. Chem.* **1957**, *29*, 916−918.
(39) Huglin, M. B. *Light Scattering from Polymer Solutions*; Academic Press: London, 1972.
(40) Pedersen, J. S. Analysis of small-angle scattering data from colloids and polymer solutions: modeling and least-squares fitting. *Adv. Colloid Interface Sci.* **1997**, *70*, 171−210.
(41) Liu, Y.; Shui, X.; Wang, M.; Zhang, C.; Wang, Y. Rational design of soluble and clickable polymers prepared by conventional free radical polymerization of acetylene-functionalized acrylate. *Polym. Chem.* **2017**, *8*, 2363−2369.

https://dx.doi.org/10.1021/acs.biomac.9b01596
Biomacromolecules 2020, 21, 955−965

(42) Aseyev, V.; Hietala, S.; Laukkanen, A.; Nuopponen, M.; Confortini, O.; Du Prez, F. E.; Tenhu, H. Mesoglobules of thermoresponsive polymers in dilute aqueous solutions above the LCST. *Polymer* **2005**, *46*, 7118−7131.
(43) Laukkanen, A.; Valtola, L.; Winnik, F. M.; Tenhu, H. Formation of Colloidally Stable Phase Separated Poly(N-vinylcaprolactam) in Water: A Study by Dynamic Light Scattering, Microcalorimetry, and Pressure Perturbation Calorimetry. *Macromolecules* **2004**, *37*, 2268−2274.
(44) Mikheeva, L. M.; Grinberg, N. V.; Mashkevich, A. Y.; Grinberg, V. Y.; Thanh, L. T. M.; Makhaeva, E. E.; Khokhlov, A. R. Microcalorimetric Study of Thermal Cooperative Transitions in Poly(N-vinylcaprolactam) Hydrogels. *Macromolecules* **1997**, *30*, 2693−2699.
(45) Maeda, Y.; Nakamura, T.; Ikeda, I. Hydration and Phase Behavior of Poly(N-vinylcaprolactam) and Poly(N-vinylpyrrolidone) in Water. *Macromolecules* **2002**, *35*, 217−222.
(46) Liu, Z.; Wickramasinghe, S. R.; Qian, X. Ion-specificity in protein binding and recovery for the responsive hydrophobic poly(vinylcaprolactam) ligand. *RSC Adv.* **2017**, *7*, 36351−36360.
(47) Sun, X.; Qian, X. Atomistic Molecular Dynamics Simulations of the Lower Critical Solution Temperature Transition of Poly(N-vinylcaprolactam) in Aqueous Solutions. *J. Phys. Chem. B* **2019**, *123*, 4986−4995.
(48) Laukkanen, A.; Wiedmer, S. K.; Varjo, S.; Riekkola, M.; Tenhu, H. Stability and thermosensitive properties of various poly (N-vinylcaprolactam) microgels. *Colloid Polym. Sci.* **2002**, *280*, 65−70.
(49) Schwarz, F. P.; Puri, K. D.; Bhat, R. G. A Surolia Thermodynamics of monosaccharide binding to concanavalin A, pea (*Pisum sativum*) lectin, and lentil (*Lens culinaris*) lectin. *J. Biol. Chem.* **1993**, *268*, 7668−7677.
(50) Mandal, D. K.; Kishore, N.; Brewer, C. F. Thermodynamics of Lectin-Carbohydrate Interactions. Titration Microcalorimetry Measurements of the Binding of N-Linked Carbohydrates and Ovalbumin to Concanavalin A. *Biochemistry* **1994**, *33*, 1149−1156.
(51) Slavík, J. Anilinonaphthalene sulfonate as a probe of membrane composition and function. *Biochim. Biophys. Acta* **1982**, *694*, 1−25.
(52) Sun, S.; Wu, P. Infrared Spectroscopic Insight into Hydration Behavior of Poly(N-vinylcaprolactam) in Water. *J. Phys. Chem. B* **2011**, *115*, 11609−11618.

https://dx.doi.org/10.1021/acs.biomac.9b01596
Biomacromolecules 2020, 21, 955−965